

# Exploring Impact of Doppler Effect on Time-Varying Multipath Wireless Communication Channels via Model Based Characteristic Analysis

ZHENGMAO YE  
College of Engineering  
Southern University  
Dcwp"Twig."NC92: 35.  
.....USA

*Abstract:* In areas of outdoor wireless communication, the Doppler shift occurs due to the relative motion between the transmitter and receiver. To apply any baseband channel model for multipath propagation, some real-world phenomena must be taken into account, such as the Doppler effect, time dispersion, and multipath scattering. Time dispersion of the radio channel leads to the Intersymbol Interference (ISI) which degrades communication performance. Scattering at diverse angles gives rise to a range of Doppler frequency shifts referred to as the Doppler spectrum. The maximum Doppler shift arises whenever the scattering direction is opposite to the channel trajectory. The Rayleigh or Rician fading distributions of the communication channel are used to characterize the line-of-sight (LOS) and non-line-of-sight (NLOS) path radio propagation, respectively. Multipath fading causes frequency-selectivity and Doppler shifting causes time-selectivity. Two popular modeling techniques for fading channels are the Filtered White Gaussian Noise and Sum-Of-Sinusoids schemes. The impact of the Doppler effect on wireless communication channel characteristics will be examined using the model based performance analysis.

*Key-Words:* Wireless Communication, Multipath Fading Channel, Doppler Effect, Rayleigh Fading, Filtered .....White Gaussian Noise Model, Sum-of-Sinusoids Channel Model0

Received: April 9, 2024. Revised: October 22, 2024. Accepted: November 23, 2024. Published: December 31, 2024.

## 1 Introduction

There are two major spatial scales of fading in wireless communication networks (e.g., wireless sensor networks, cellular networks): large scale fading (path loss, shadowing, penetration) and small scale fading (LOS, NLOS). In fact channel fading is superimposed upon large-scale and small-scale effects. The Doppler effect could be constructive or destructive for multipath fading up with respect to critical distances. The focus of this research instead is on the small-scale effect, covering reflections, scattering, and diffraction. Whenever there is a dominating line of sight (LOS) from the transmitter to the receiver, Rician fading is most applicable. Without a dominating line of sight instead, Rayleigh fading is most applicable for non-LOS propagation. It is a special case of two-wave channel with diffuse power fading. On the other hand, the Rayleigh distribution is formulated by taking two independent and identically distributed (IID) zero mean Gaussian random variables as real and imaginary parts of a complex number. The random fading process has zero mean and evenly phase distribution between 0 and  $2\pi$  radians. The envelope of the communication channel magnitude response manifests the Rayleigh distribution, which turns out to be the radial

component of the sum of two uncorrelated Gaussian random variables. Actually Rayleigh fading acts as the small-scale effect, the fading instead contains bulk properties of the environment where both path loss and shadowing are superimposed. For small scale fading, potential multi-path fading produces frequency selectivity with the coherence bandwidth. The Doppler effect is specified in terms of the relative speed between the transmitter and receiver, and the Doppler shift produces time-selectivity with coherence time. The Doppler spread is a measure of the spectral broadening caused by the time rate of change of the mobile radio channel, and it is defined as the range of frequencies over which the received Doppler spectrum is essentially non-zero. The standard deviation of multiple spectral shifts is related to the Doppler spread, which reflects the change in the carrier frequency [1], [2].

Wireless sensor networks (WSNs) serve as the popular media of communication between the transmitters and receivers. Research on WSNs is challenging where combination of computing, sensing, control and communication technologies is necessary. For example, a Zone Efficient Localized Data Aggregation scheme is proposed to reduce energy consumption and routing traffic needed

using data funneling techniques. Topology control of the wireless sensor networks via integration of Kalman filters and adaptive estimation is proposed for wireless sensor networks design. Path loss modeling for large scale fading shows the tradeoff between range and bandwidth. Maxwell equations provide perfect analytical models for the path loss however too complex to be practical. Empirical models have the limit functionality against various environments and Ray tracing models require site-specific information. The simple free space path loss models are instead most practical. Several path loss models are analyzed to predict the attenuation performance upon parameter variations. The power control strategy based on Signal to Interference plus Noise Ratio (SINR) balancing is shown to minimize power consumption and optimize power control in wireless cellular networks [5]. WSNs employ the battery-powered sensor nodes for sensing, so the lifespan depends on the energy efficiency. There is always a trade-off among energy consumption, latency and reliability. Dynamic clustering based routing is proposed to achieve good performance via adaptive algorithms. The best practical dynamic routing technique is analyzed and synthesized [6], [7]. A statistical channel model covers two components with random phases and a diffuse component. This fading model provides better match than Rician fading of recent small-scale fading measurements in 28 GHz outdoor channels. Its performance is evaluated in terms of the bit error rate and the outage capacity, and the interplay between fading model parameters. Monte Carlo simulations are carried out to validate the obtained theoretical expressions [8]. Statistical characterization of SINR is critical in study of cellular networks, to capture diverse fading channels arising in realistic outdoor and indoor wireless communication scenarios. By exploiting moment generating function of the SINR, cellular network performance is estimated over the shadowed  $\kappa$ - $\mu$ ,  $\kappa$ - $\mu$ , and  $\eta$ - $\mu$  fading models. The channel models show high flexibility by applying diverse fading channels, such as the models with Rayleigh, Nakagami, Rician, and Rician shadow fading distributions. The coverage, achievable rate, and bit error probability are integrated [9].

Impact of scalability and density on the lifespan of WSNs is analyzed and synthesized, which depends on the sensor node deployment. Scalability is closely relevant to the connectivity and coverage range of WSNs, which in turn determines the WSNs lifespan. Single-hop routing is more efficient for WSNs in the small diameter coverage range at the high radio transceiver power. It is chosen for sensor deployment analysis under diverse density and

scalability [10]. Emerging cellular technologies for 5G communications are confronted with a wide range of usage and diverse link requirements. To bridge the gaps between theoretical and practical channels, the  $\kappa$ - $\mu$  shadowed fading is presented. Parameters of a heterogeneous cellular network are evaluated with  $K$  classes of the base stations (BSs), differing with respect to transmit power, shadowing, fading characteristics and BS density [11]. The 5G cellular systems will operate in a broad frequency range, with extra mm-wave frequency bands, at single band or multiple bands simultaneously. The pathloss, shadow fading, root-mean-square (RMS) delay spreads, Rician factor and coherence bandwidth are all characterized in urban macro-cellular and micro-cellular environments. By dividing a wideband channel transfer function into subbands of 1 GHz bandwidth each, the relevant frequency dependence is studied in the 3–18 GHz band. The shadow fading and Rician factor increase with frequency. The RMS delay spread decreases in LOS environments with frequency, but varies little in NLOS propagation. The coherence bandwidth changes slightly with frequency [12]. The RIS (Reconfigurable Intelligent Surface) empowered communication is the promising 6G technology which converts a wireless channel to an intelligent transmit entity by manipulating impinging waves using manmade surfaces. The potential benefits of RISs are examined via indoor and outdoor models across broadband. The path loss exponent has been analyzed using the empirical path loss models. Transmission models with multiple RISs are analyzed and synthesized for indoor and outdoor NLOS scenarios. Simulation results demonstrated that it provides promising solutions for indoor and outdoor cases at various operating frequencies. It also shows improvement of error performance and achievable data rates even in presence of system imperfections like limited range phase adjustment and imperfect phase estimation at RISs [13].

## 2 Fundamentals of Small Scale Multi-Path Fading Channel

The outdoor wireless communication channel is typically characterized by Doppler spectrum which governs the time variation in the channel gain, which fluctuates rapidly over time. Without loss of generality, some popular small scale multi-path fading channel models are selected to examine the impact of Doppler shifts on fading characteristics. Except for the computational complex baseline filtered white Gaussian noise (FWGN) model, other

popular models widely applied including the FWGN model in time domain, modified FWGN model in frequency domain, and Jakes standardized sum-of-sinusoids model.

Linear time-varying systems can be simply introduced to describe the input output relationship for outdoor wireless communication channels. Let  $x(t)$  be the baseband transmit signal in the electromagnetic field with  $N$  planewaves of the average power. Doppler shifts occur among all planewaves with diverse arrival angles and arbitrary carrier phases. The corresponding passband transmit signal is shown as (1):

$$\hat{x}(t) = \text{Re} [x(t)e^{j\omega_c t}] \quad (1)$$

where  $\text{Re}[\cdot]$  refers to the real component,  $\omega_c = 2\pi f_c$  is the carrier angular frequency. A scattered channel covers  $N$  individual propagation paths with different Doppler shifts. Then the received signal is expressed as (2).

$$\hat{y}(t) = \text{Re} [y(t)e^{j\omega_c t}] = \text{Re} \left[ \sum_{i=1}^N C_i e^{j(\omega_c + \omega_i)(t - \tau_i)} x(t - \tau_i) \right] \quad (2)$$

where  $C_i$ ,  $\tau_i$ , and  $\omega_i = 2\pi f_i$  represent the channel gain, path delay and angular Doppler shift for the  $i$ -th propagation path, respectively. The corresponding baseband received signal is formulated as (3):

$$y(t) = \sum_{i=1}^N C_i e^{-j\phi_i(t)} x(t - \tau_i) \quad (3)$$

Now a linear time-varying filter is brought in to model the channel with complex baseband impulse response:

$$h(t, \tau) = \sum_{i=1}^N C_i e^{-j\phi_i(t)} \delta(t - \tau_i) \approx h(t) \delta(t - \hat{\tau}) \quad (4)$$

where  $\delta(\cdot)$  is the unit impulse function or Dirac delta function. When the path delay mismatch is much shorter than the sampling time, each path delay  $\tau_i$  can be approximated as  $\tau$ . So (4) has been simplified as (5) and (6).

$$h(t, \tau) = h(t) \delta(t - \tau) \quad (5)$$

$$h(t) = \sum_{i=1}^N C_i e^{-j\phi_i(t)} \quad (6)$$

Given the normalized baseband transmit causal signal  $x(t) = 1$ . It represents the unit step function, the received passband signal  $y(t)$  can then be simplified as (7) accordingly.

$$\begin{aligned} \hat{y}(t) &= \text{Re} [y(t)e^{j\omega_c t}] \\ &= \text{Re} [\{h_1(t) + jh_Q(t)\} e^{j\omega_c t}] \\ &= h_1(t) \cos \omega_c t - h_Q(t) \sin \omega_c t \end{aligned} \quad (7)$$

where  $h_1(t)$  and  $h_Q(t)$  refer to the in-phase and quadrature components of  $h(t)$ , respectively, which are formulated in (8).

$$h_1(t) = \sum_{i=1}^N C_i \cos \phi_i; \quad h_Q(t) = \sum_{i=1}^N C_i \sin \phi_i \quad (8)$$

If  $N$  is large enough, by the central limit theorem,  $h_1(t)$  and  $h_Q(t)$  can both be represented by Gaussian random variables.

For the complex Gaussian random variables, the corresponding magnitude of the received signal exhibits the Rayleigh distribution, which is subject to diverse scattering in a multipath channel. In general, propagation environment for the outdoor wireless channel is under the NLOS environment. The corresponding power spectrum density (PSD) of the fading process can be formulated by the Fourier transform of the autocorrelation function of the received passband signal known as the classical Doppler spectrum (9), where  $f_D$  is the maximum Doppler frequency and  $f_c$  is the carrier frequency.

$$S(f) \propto \frac{1}{\sqrt{1 - \left(\frac{f - f_c}{f_D}\right)^2}} \quad |f - f_c| \leq f_D \quad (9)$$

### 3 Multi-Path Fading Channel Models

The Doppler effect plays a major role in wireless fading channel characteristics. When the scattering components have the propagation direction exactly opposite to the signal trajectory, the maximum Doppler shift arises. In general there are 2 main fading channel modeling techniques for path gains of channel filters: either the FWGN technique or sum of sinusoids modeling technique. As for the former technique, a complex uncorrelated Gaussian random process with zero mean and normalized variance is generated in the discrete time. A Doppler filter is then applied via the desired Doppler power spectrum. Interpolation and extrapolation can both be implemented to be consistent with the existing sample period of input signals. As for the latter one, the uncorrelated Rayleigh fading waveforms are superimposed independently to produce both in-phase and quadrature components.

#### 3.1 Time-Domain FWGN Model

The time-domain Filtered White Gaussian Noise (FWGN) channel model is straightforward and flexible. Duration of fading channel is simply determined by the length of a complex Gaussian random signal generated in the time-domain. The block diagram of the time domain FWGN model is shown in Fig. 1. The complex Gaussian random signal can be easily generated in the discrete time-domain. Also the number of complex Gaussian random samples can be increased or decreased by

adjusting the simulation interval with flexibility, with a tradeoff of computational complexity. The Doppler filter is applied afterwards to generate the Doppler-shifted Gaussian noise. Implementation of the Doppler filter is made by an FIR filter to avoid instability, whose impulse response coefficients can be computed by inverse Fourier transform of the power spectral density function of classical Doppler spectrum, while other types of the Doppler spectrum can also be applied, like the flat Doppler spectrum.



Fig. 1 Block Diagram of Time Domain Filtered White Gaussian Noise (FWGN) Model

### 3.2 Frequency-Domain FWGN Model

The basic idea of the frequency domain Filtered White Gaussian Noise (FWGN) channel model is to construct two uncorrelated separate branches to represent the real part and imaginary part of complex channel gain completely independent of each other. With the assumption of isotropic scattering, the Rayleigh fading model has been accomplished by simulating two uncorrelated zero mean Gaussian random variables. In Fig.2, the block diagram of the frequency domain FWGN model is shown. Initially the complex Gaussian white noise is generated in the frequency domain. The Doppler shift is then applied to complex Gaussian white noise as the Doppler filters. The input should be conjugate symmetric always, so that after inverse Fourier transform is applied, the total superimposed output from two branches of the Doppler-shifted Gaussian noise will give rise to a real time-domain signal. The overall time-varying channel gain is determined to have the Rayleigh distribution in amplitude and uniform distribution in phase.

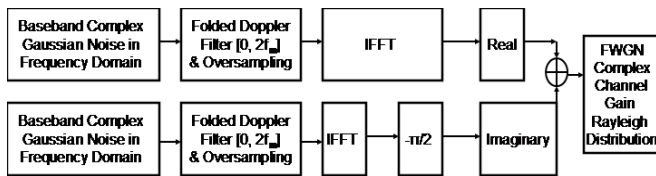


Fig. 2 Block Diagram of Frequency Domain Filtered White Gaussian Noise (FWGN) Model

To reduce the computational complexity, an alternative in the frequency domain can be applied. In the frequency-domain, let  $f_D$  be the maximum Doppler frequency. The spectrum repeats with respect to Nyquist frequency  $2f_D$ . Now folding from a symmetric frequency band  $[-f_D, f_D]$  to a positive frequency band  $[0, 2f_D]$  is needed for conducting

inverse Fourier transform, as shown in 2<sup>nd</sup> block of Fig. 2. Here the positive and negative frequency correspond to the counterclockwise and clockwise angular direction, respectively. The actual count of discrete-frequency samples within scope of Doppler bandwidth, is determined by the number of samples in the fading channel and the extra oversampling factor. It makes it possible to generate the fading signal with the specified overall channel length without taking maximum Doppler frequency into account. By applying a uniform phase onto the Doppler filter, it results in the more flexible way to describe the channel fading process.

### 3.3 Standardized Sum-of-Sinusoids Model

The Jakes channel model is the standardized Sum of Sinusoids model. Its block diagram is shown in Fig. 3. The Rayleigh fading channel with a specified Doppler spectrum has been generated by synthesizing complex sinusoids. The number of sinusoids must be big enough to approximate the Rayleigh amplitude. For isotropic scattering, the receiver collects rays of the scattered components from all directions of N plane waves with an evenly distributed spacing of  $2\pi/N$ .

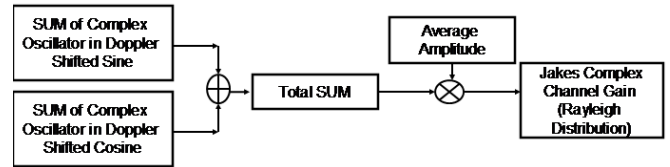


Fig. 3 Block Diagram of Jakes Channel Model

The weighted sinusoidal generators are used to produce the desired Doppler spectrum. The real and imaginary parts,  $h_I(t)$  and  $h_Q(t)$  in the total sum of the complex oscillators are:

$$h_I(t) = 2 \sum_{n=1}^{N_0} \cos \phi_n \cos \omega_n t + \sqrt{2} \cos \phi_{N_0} \cos \omega_{d_0} t \quad (10)$$

$$= 2 [\cos \phi_1 \cdots \cos \phi_{N_0} \cos \phi_{N_0}] [\cos \omega_1 t \cdots \cos \omega_{N_0} t \cos \omega_{d_0} t / \sqrt{2}]^T$$

$$h_Q(t) = 2 \sum_{n=1}^{N_0} \sin \phi_n \cos \omega_n t + \sqrt{2} \sin \phi_{N_0} \cos \omega_{d_0} t \quad (11)$$

$$= 2 [\sin \phi_1 \cdots \sin \phi_{N_0} \sin \phi_{N_0}] [\cos \omega_1 t \cdots \cos \omega_{N_0} t \cos \omega_{d_0} t / \sqrt{2}]^T$$

where  $\Phi_n$  and  $\Phi_{N_0}$  are the initial phases of the n-th Doppler-shifted sinusoid,  $f_D$  is the maximum Doppler frequency. The initial phase can be set to  $\pi n / (N_0 + 1)$  and 0, which satisfies the uniform distribution. The complex output of the Jakes model is represented as (12).

$$h(t) = \frac{E_0}{\sqrt{2N_0 + 1}} \{h_I(t) + j h_Q(t)\} \quad (12)$$

where  $E_0$  is the average amplitude of the fading channel.  $E_0^2$  is the average power of the fading channel. The real and imaginary parts of the channel are statistically independent, sharing the average power of  $E_0^2/2$  each, as shown in (13-15).

$$E\{h(t)\} = E_0 \quad (13)$$

$$E\{h_I(t)h_Q(t)\} = 0 \quad (14)$$

$$E\left\{\left(\frac{E_0 h_I(t)}{\sqrt{2N_0+1}}\right)^2\right\} = E\left\{\left(\frac{E_0 h_Q(t)}{\sqrt{2N_0+1}}\right)^2\right\} = \frac{E_0^2}{2} \quad (15)$$

## 4 Time Domain Analysis

The time-domain characteristics of the multipath Doppler shifted frequency flat fading channel can be analyzed via various models (e.g. baseline FWGN model). The time-varying channel gain will exhibit the Rayleigh distributed amplitude and uniformly distributed phase. The increment of Doppler shift causes more rapid variations in channel amplitude, which can lead to the fast fading characteristics. Without any LOS component, multipath frequency selective fading in wireless communication channels can also be modeled as the Rayleigh distribution. In case that different Doppler spectra occur in multiple paths with totally diverse levels of the maximum Doppler shifts, both the amplitude distribution and phase distribution are subject to distortion and even impairment. The impact of the Doppler shifts on multipath characteristics are analyzed via numerical simulations using typical models. The comparisons on the Doppler impact are made in terms of the path channel gain characteristics as well as distributions of both the magnitude and phase.

The 5-path frequency-selective fading channel is chosen with the fixed sampling period of  $5 \mu\text{s}$ . The maximal Doppler frequency is assumed to be 50 Hz, 100 Hz, 200 Hz, 500 Hz and 1 KHz, respectively. As the maximum Doppler frequency across 5 paths varies from 50 Hz to 1000 Hz, the impact of the Doppler shift on each individual path also varies dramatically. Simulations on characteristic changes from slow fading to fast fading are thus conducted.

For the time domain FWGN model, the time-varying channel gains of 5 paths are shown in Fig. 4. In general, the envelopes of individual gain amplitude retain the Rayleigh distribution however subject to distortion. The lower the maximum Doppler frequency, the higher the distortion in that path. On the other hand, the phase characteristics still retain uniform distribution only in those paths with large maximum Doppler frequencies, while phase characteristics no longer follow the uniform

distribution in paths with small maximum Doppler frequencies instead.

For the frequency domain FWGN model, the time-varying channel gain is shown in Fig. 5. In general, the amplitude and phase characteristics still retain Rayleigh distribution and uniform distribution in those paths with large maximum Doppler frequencies. In paths with the smallest maximum Doppler frequency, the amplitude characteristics and phase characteristics fail to follow the Rayleigh distribution and uniform distribution. At the lowest Doppler shift of 50 Hz under fixed sampling period, the coherence time is much larger than the symbol period. The signal bandwidth is much broader than the channel bandwidth. Typical characteristics of frequency selective is observed. At the same time, the channel variation is much slower than that of baseband signal. It has a narrow Doppler spread and the coherence time is much greater than the symbol period, indicating very slow fading, which has the largest impact on frequency selective fading channel characteristics.

For the Jakes sum of sinusoids channel model, the time-varying channel gain is shown in Fig. 6. In general, the patterns of amplitude characteristics in all 5 paths still retain Rayleigh distribution, however minor changes can be observed for paths with smallest maximum Doppler frequencies. On the other hand, the patterns of phase characteristics in all 5 paths retain uniform distribution, no matter in any path from the smallest to largest maximum Doppler frequency.

Comparing three sets of results, it is observed that Jakes channel model is the best option to describe the Doppler spectrum. The time domain FWGN model is slightly better than the frequency domain FWGN model.

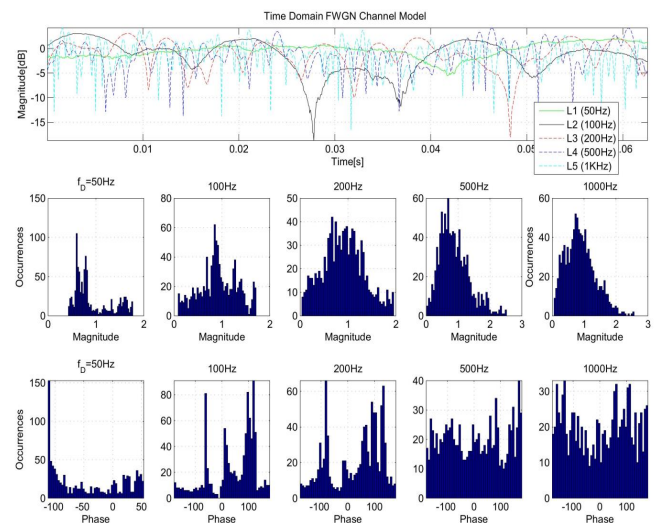


Fig. 4 Time Domain FWGN Channel Model

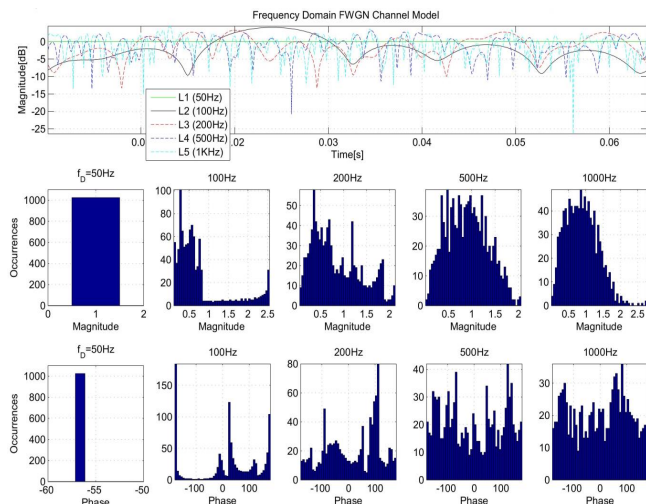


Fig. 5 Frequency Domain FWGN Channel Model

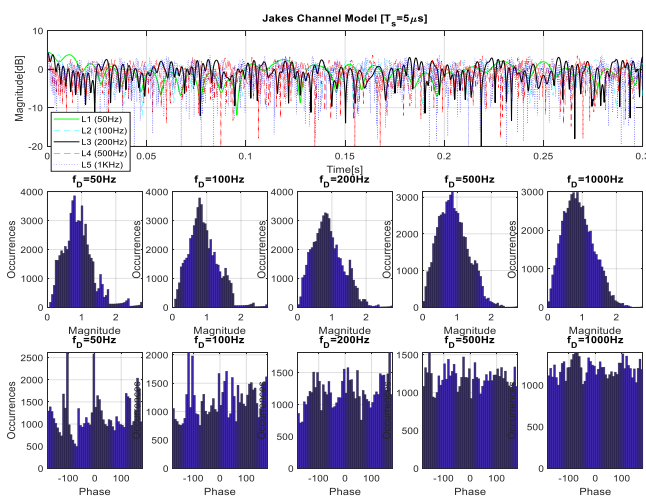


Fig. 6 Sum-of-Sinusoids (Jakes) Channel Model

## 5 Doppler Spectrum Analysis

In this session, comparisons of 3 typical models are made in terms of the autocorrelation function and Doppler spectrum.

The impulse response of the channel is correlated as a power-delay profile. The power delay profile plots the received signal power across multipath as a function of propagation delays of individual paths. Autocorrelation represents the degree of similarity between a time sequence and its delayed sequence over successive time intervals. It measures the relevance between present values and past values in order to predict future values. Instead of the correlation defined between two different time series, the autocorrelation focuses on the same time series twice. The power spectral density (PSD) or power spectrum of a stationary random process is nothing but Fourier transform of the autocorrelation function. It is the measure of the signal power

distribution over frequency. When the signal is real, its PSD is real and even, similar to autocorrelation functions. The popular classical Doppler spectrum is defined with respect to the power spectral density function. The 5-path frequency-selective fading channel is chosen with a fixed sampling period of 5  $\mu$ s again. The Doppler frequency is assumed to be 50 Hz, 100 Hz, 200 Hz, 500 Hz and 1 KHz across 5 paths, respectively. Autocorrelation in terms of time delays and the power spectral density function in terms of normalized frequency should be analyzed accordingly.

For the time domain FWGN channel model, the time-varying channel gain is illustrated in Fig. 7, together with the classical and simulated Doppler spectra and autocorrelation functions. The higher the maximum Doppler frequency, the larger the mismatch on the channel gain between the classical and simulated Doppler spectra in that path. In addition, inside the positive frequency between  $[0, 2f_D]$ , the higher the maximum Doppler frequency, the larger in that path the mismatch between autocorrelation functions of classical and simulated Doppler spectra. In fact an autocorrelation of +1 represents perfect positive correlation, while an autocorrelation of -1 represents perfect negative correlation.

For the frequency domain FWGN channel model, the time-varying channel gain is illustrated in Fig. 8, together with the classical and simulated Doppler spectra and autocorrelation functions. Similar results are obtained on channel gain as those in the time domain FWGN model. The higher the maximum Doppler frequency, the larger the mismatch on the channel gain between the classical and simulated Doppler spectra in that path. Once again inside the positive frequency between  $[0, 2f_D]$ , relatively larger mismatches on autocorrelations have been observed than those in the time domain FWGN model across all ranges of the maximum Doppler frequency.

For the Jakes channel model, the time-varying channel gain is illustrated in Fig. 9, together with the classical and simulated Doppler spectra and autocorrelation functions. The higher the maximum Doppler frequency, the larger mismatch between the simulated and theoretical results in that path. Within the symmetrical frequency band between  $[-f_D, f_D]$ , the higher the normalized frequency in a path, the larger mismatch of the autocorrelation functions between the simulated and theoretical results. For a special numerical simulation case at a low Doppler shift of 50 Hz, U-shape classical Doppler spectrum is mostly replaced by symmetric piecewise linear functions, indicating the narrow Doppler spread. It demonstrated that in general the Jakes channel

model outperforms the FWGN channel models on Rayleigh distribution implementations with better matches on the autocorrelation functions and power spectral density functions.

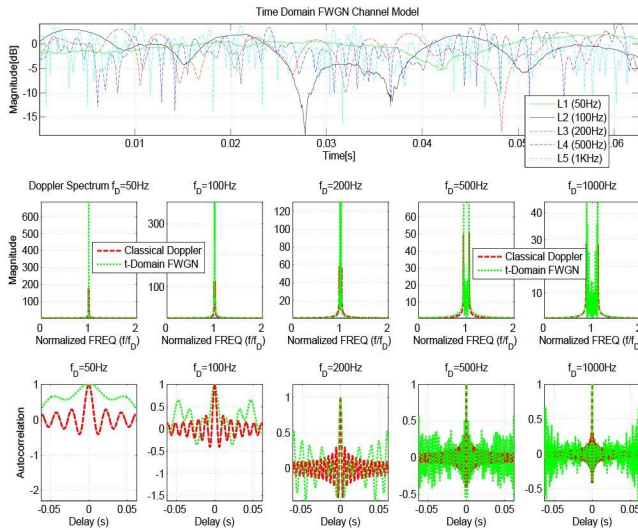


Fig. 7 Time Domain FWGN Channel Model

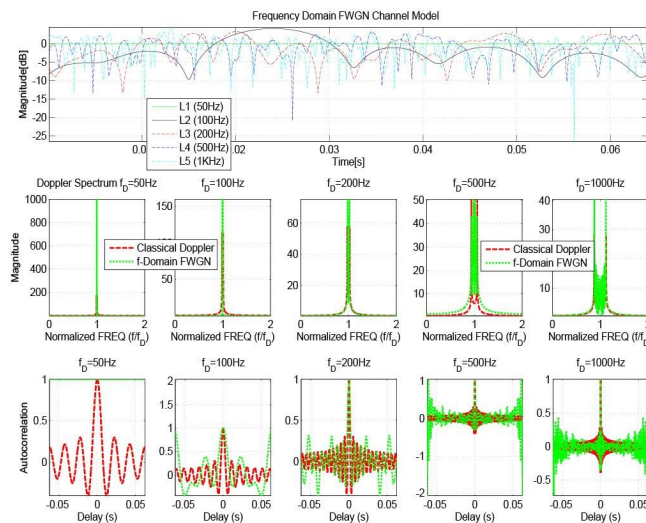


Fig. 8 Frequency Domain FWGN Channel Model

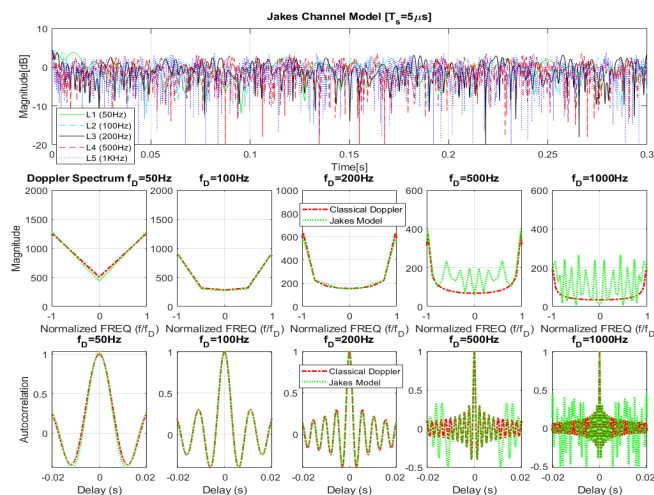


Fig. 9 Sum-of-Sinusoids (Jakes) Channel Model

## 6 Conclusion

In outdoor wireless communication, path loss models and shadowing are applied to compute large scale attenuations. Instead the Rayleigh and Rician fading channel models are applied to describe small scale attenuations. Meanwhile Rayleigh fading is widely used in the dense downtown areas with rich scattering. Independent propagation mechanisms involve in time dispersion and frequency dispersion, respectively. In multipath fading channels, the delay spread causes frequency-selective fading and time dispersion, while the Doppler spread causes time-selective fading and frequency dispersion. Thus it is necessary to encompass both frequency selectivity and time selectivity in the time-varying multipath fading models. Via time domain analysis, the power delay profiles, the magnitude distribution and phase distribution have been compared in detail across a broad range of Doppler shifts. Also via Doppler spectrum analysis, the Doppler power spectrum density and autocorrelation functions have been examined across a broad range of Doppler shifts. Rayleigh fading channel models are capable of giving close approximations for the real world multipath fading channels. Based on the numerical analysis and synthetics, the time domain FWGN model slightly outperforms the frequency domain FWGN model to represent the classical Doppler spectrum with respect to both magnitude and phase distributions as well as autocorrelation functions. The standardized sum of sinusoids model instead provides best approximations among three popular schemes to represent complex Doppler spectra, experiencing the least impact from the Doppler frequency shift.

### References:

- [1] B. Lathi, Z. Ding, "Modern Digital and Analog Communication Systems", Fourth Edition, Oxford University Press, 2009
- [2] R. Schilling, S Harris, "Fundamental of Digital Signal Processing Using Matlab", First Edition, Cengage Publishing, 1990
- [3] S. Bhatte, H. Majlesein, Z. Ye, H. Mohamadian, "Development of Novel Wireless Sensor Networks and Potential Optimization via Kalman Filtering", 2009 IEEE Conference on Industrial Electronics and Application, pp. 3983-3988, May 25-27, 2009, XiAn, China
- [4] Z. Ye and H. Mohamadian, "WSN Topology Control Design via Integration of Kalman Filtering and Adaptive Estimation", Proceedings of 2009 International Conference on Electrical

- Engineering, Computing Science and Automatic Control, pp. 41-45, NOV 10-13, 2009, Mexico
- [5] Z. Ye and H. Mohamadian, "Comparative Study of Path Loss Models for Wireless Cellular Networks and Optimal Power Control with Respect to SINR Balancing", *Journal of Information Systems Technology and Planning*, pp. 1-13, Volume 6, Issue 16, 2013
- [6] Z. Ye and H. Mohamadian, "Adaptive Clustering Based Dynamic Routing of Wireless Sensor Networks via Generalized Ant Colony Optimization", *Proceedings of 2014 International Conference on Future Information Engineering*, July 7-8, 2014, Beijing, China
- [7] Z. Ye, "Analysis and Synthesis of Vehicle Routing Problems Using Heuristic and Exact Algorithms for Transportation Combinatorial Optimization", *2023 International Conference on Electrical Engineering, Computing Science and Automatic Control*, OCT 25-27, 2023, Mexico City, Mexico
- [8] J. Romero-Jerez, F. Lopez-Martinez, P. Javier, F. Jose, A. Goldsmith, "The Fluctuating Two-Ray Fading Model: Statistical Characterization and Performance Analysis", *IEEE Transactions on Wireless Communications*, V16, N7, pp. 4420-4432, July 2017
- [9] I. Trigui, S. Affes, B. Liang, "Unified Stochastic Geometry Modeling and Analysis of Cellular Networks in LOS/NLOS and Shadowed Fading", *IEEE Transactions on Communications*, v 65, n 12, p 5470-86, DEC 2017
- [10] Z. Ye, H. Yin, and Y. Ye, "Impact of Scalability and Density on Lifespan of Energy-Efficient Wireless Sensor Networks", *2020 International Scientific and Practical Conference on Information Control Systems and Technologies*, September 24-26, 2020, Odessa, Ukraine
- [11] J. Young, S. Cotton, H. Dhillon, J. Lopez-Martinez, J. Paris, K. Seong, "A Comprehensive Analysis of 5G Heterogeneous Cellular Systems Operating over  $\kappa$ - $\mu$  Shadowed Fading Channels", *IEEE Transactions on Wireless Communications*, v 16, n 11, p 6995-7010, Nov. 2017
- [12] V. Kristem, C. Bas, R. Wang, A. Molisch, "Outdoor Wideband Channel Measurements and Modeling in 3–18 GHz Band", *IEEE Transactions on Wireless Communications*, v 17, n 7, p 4620-33, July 2018
- [13] I. Yildirim, A. Uyrus, E. Basar, "Modeling and Analysis of Reconfigurable Intelligent Surfaces for Indoor and Outdoor Applications in Future Wireless Networks", *IEEE Transactions on Communications*, v69, p1290-1301, FEB 2021

### **Contribution of Individual Authors to the Creation of a Scientific Article (Ghostwriting Policy)**

The author contributed in the present research, at all stages from the formulation of the problem to the final findings and solution.

### **Sources of Funding for Research Presented in a Scientific Article or Scientific Article Itself**

No funding was received for conducting this study.

### **Conflict of Interest**

The author has no conflict of interest to declare that is relevant to the content of this article.

### **Creative Commons Attribution License 4.0 (Attribution 4.0 International, CC BY 4.0)**

This article is published under the terms of the Creative Commons Attribution License 4.0

[https://creativecommons.org/licenses/by/4.0/deed.en\\_US](https://creativecommons.org/licenses/by/4.0/deed.en_US)